Efficient Finite Element Analysis of Axially Symmetrical Waveguides and Waveguide Discontinuities

Malgorzata Warecka, Rafal Lech, *Senior Member, IEEE,* and Piotr Kowalczyk, *Member, IEEE*

Abstract—A combination of the body-of-revolution and finite element methods is adopted for full-wave analysis of waveguides and waveguide discontinuities involving angular field variation. Such an approach is highly efficient and much more flexible than analytical techniques. The method is performed in two different cases: utilizing a generalized impedance matrix to determine the scattering parameters of a single waveguide section, and utilizing periodic boundary conditions without sources. In order to confirm the validity and efficiency of both approaches a few examples of axially symmetrical structures have been analyzed. The obtained results are compared to those obtained from commercial software and available in the literature.

Index Terms—Cylindrical waveguides, Dispersion diagrams, Finite element method, Generalized impedance matrix, Meta-materials, Periodic boundary conditions.

I. Introduction

AXIALLY symmetrical structures (see. Fig. 1) have been widely used in microwave technology and optics for many years. For instance, cylindrical waveguides containing different types of discontinuities are commonly applied in passive filtering devices [1]–[4]. In the last few decades, periodic structures known as electric or photonic band-gap materials have also become very popular due to their wide practical applications. Such structures can support left-handed waves as well as backward and slow waves. The specific properties of these systems can be utilized for miniaturization of waveguides or modification of their operating band [5]–[9]. Special attention should also be given to their application in electron beam devices such as gyrotrons, magnetrons, travelling-wave tubes, backward-wave oscillators, gyro-travelling-wave tubes and accelerators, where the structure is composed of periodic metal-dielectric layers [10], [11]. The interaction of an electron beam with the fields supported in a slow-wave structure gives these structures potential for THz devices.

For a structure with a simple geometry an analytical method (e.g. mode matching) can be applied [7], [8], however in

M. Warecka, R. Lech and P. Kowalczyk are with the Department of Microwave and Antenna Engineering, Faculty of Electronics, Telecommunications and Informatics, Gdansk University of Technology, Gdansk 80-233, Poland (e-mail: warecka.malgorzata@gmail.com, rlech@eti.pg.edu.pl, pio.kow@gmail.com.)
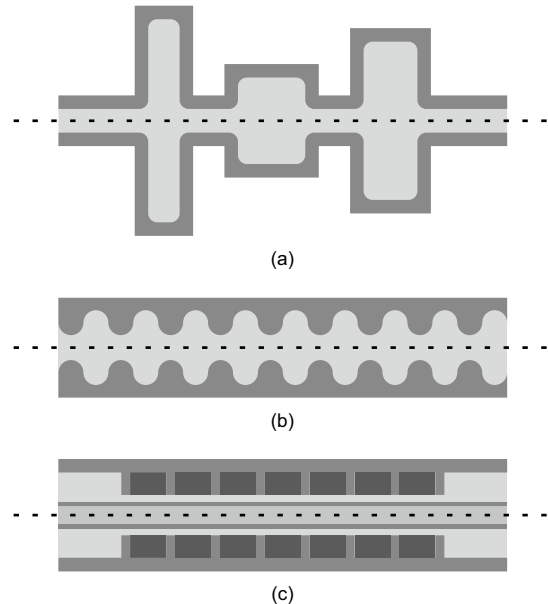
Fig. 1. Axial cross section of (a) Microwave filter (b) Slow-wave periodic structure (c) Circular waveguide with electron beam.

many practical cases such an approach is not sufficiently flexible. More sophisticated techniques, e.g. boundary integral-resonant-mode expansion (BI-RME) [12], [13], can be used for more complicated geometries, however their application is less general than discrete numerical techniques, which have recently become the most popular analysis methods. Usually, commercial full-wave simulators based on the finite difference (FD) or finite element method (FEM) require a discretization of the whole three dimensional computational domain inside the structure. For complex geometries, especially containing thin metal-dielectric layers, the discretization must be fine, which results in time and memory-consuming analysis. In such cases the optimization of the structure (which requires many simulations for different parameters) can be inefficient.

It is well known that the structures of axial symmetry can be analyzed much more simply, taking advantage of the fixed angular variation of the fields - Body-Of-Revolution (BOR). This feature is widely described in the literature and applied for many different issues involving radiation, propagation and scattering problems [5], [14]–[20], and for FEM [21]–[31]. However, to the authors' best knowledge, the BOR approach for periodic and quasi-periodic guiding structures

has not been presented in combination with FEM. A recently published paper [6] considers this problem only for the case with no angular variation (suggesting that the generalization to arbitrary variation is not possible) which is useless from a practical point of view.

In this paper, a combination of BOR and FEM is adopted for full-wave analysis of waveguides and waveguide discontinuities (involving angular field variation, in opposite to [6]). Such an approach is highly efficient and much more flexible than analytical techniques. The proposed method is performed in two different cases. The first involves a generalized impedance matrix (GIM) to determine the scattering parameters of a single waveguide section. Such results can be used to analyze structures composed of the same or different sections (involving quasi-periodic or even periodic structures). The second method, based on periodic boundary conditions and no sources (modal analysis), can be applied to periodic structures, and becomes more efficient than the first for short and complex sections.

In order to confirm the validity and efficiency of both approaches, a few examples of axially symmetrical structures have been analyzed. The obtained results have been compared with those obtained from commercial software and available in the literature.

It is worth noting that the proposed approach can be easily combined with techniques which can significantly improve the efficiency of the analysis and optimization process. One example is the model order reduction [32], which is useful when the analysis is performed in a wide frequency band. Another example is based on a hybridization of the FEM with modal expansion techniques and utilizing surface impedance. If the structure involves homogeneous regions, then the field inside these regions can be expressed in analytical terms, which also improves the efficiency of the simulation [6], [33], [34]. Moreover, in the optimization process mesh morphing algorithms [35] can be applied to avoid step changes in the results caused by slight modifications of the generated mesh for different simulation parameters.

II. FORMULATION OF THE PROBLEM

Symmetric structures have some special features that can be used to improve the efficiency of analysis. In this article, a section of a cylindrical waveguide with a symmetry axis is considered. In this case, the structure can be analyzed in cylindrical coordinates in a two dimensional domain (ρ, φ) which is "rotated" around the mentioned axis (see Fig. 2). The variation of the electric (and magnetic) field along φ can be expressed as

$$\vec{E}(\rho, \varphi, z) = \vec{E}(\rho, z)e^{jm\varphi}, \tag{1}$$

where m is an arbitrary integer number (mode number). For the investigated axially symmetrical structures the analysis can be performed separately for each m.

In the first step, the fields must be separated into two components $\vec{E}_\varphi(\rho, z) = E_\varphi(\rho, z)\vec{i}_\varphi$ and $\vec{E}_t(\rho, z) = E_\rho(\rho, z)\vec{i}_\rho +$

$E_z(\rho, z)\vec{i}_z$. Then, directly from the Maxwell equations one obtains:

$$\vec{\nabla}_t \times \left(\mu_r^{-1}\vec{\nabla}_\varphi \times \vec{E}_t\right) + \vec{\nabla}_t \times \left(\mu_r^{-1}\vec{\nabla}_t \times \vec{E}_\varphi\right)$$
$$-k_0^2\varepsilon_r\vec{E}_\varphi = 0 \tag{2}$$

and

$$\vec{\nabla}_t \times \left(\mu_r^{-1}\vec{\nabla}_t \times \vec{E}_t\right) + \vec{\nabla}_\varphi \times \left(\mu_r^{-1}\vec{\nabla}_t \times \vec{E}_\varphi\right)$$
$$+\vec{\nabla}_\varphi \times \left(\mu_r^{-1}\vec{\nabla}_\varphi \times \vec{E}_t\right) - k_0^2\varepsilon_r\vec{E}_t = 0 \tag{3}$$

where the operators $\vec{\nabla}_t = \vec{i}_\rho\frac{\partial}{\partial\rho} + \vec{i}_z\frac{\partial}{\partial z}$ and $\vec{\nabla}_\varphi = \vec{i}_\varphi\frac{\partial}{\partial\varphi}$. The relative permittivity and permeability of the structure are represented by ε_r and μ_r, respectively, and k_0 is a vacuum wavenumber. A weak form of the considered problem can be obtained (similarly to [33], [34]), taking into account assumption (1), for scalar component $E_\varphi(\rho, z)$

$$-\iint_S \frac{jm}{\rho}\left[\vec{\nabla}_t(\rho F_\varphi) \cdot \mu_r^{-1}\vec{E}_t\right] \, d\rho dz$$

$$-k_0^2\iint_S \rho F_\varphi\varepsilon_r E_\varphi \, d\rho dz$$

$$+\iint_S \frac{1}{\rho}\left[\left(\vec{\nabla}_t(\rho F_\varphi)\right) \cdot \left(\mu_r^{-1}\vec{\nabla}_t(\rho E_\varphi)\right)\right] \, d\rho dz$$

$$+j\omega\mu_0\sum_{p=1}^2 \int_{L_p} F_\varphi(\vec{i}_\varphi \times \vec{H}_t^p) \cdot \vec{i}_p\rho d\rho = 0 \tag{4}$$

and for vector component $\vec{E}_t(\rho, z)$

$$\iint_S \rho(\vec{\nabla}_t \times \vec{F}_t) \cdot (\mu_r^{-1}\vec{\nabla}_t \times \vec{E}_t) \, d\rho dz$$

$$-k_0^2\iint_S \rho\vec{F}_t \cdot \varepsilon_r\vec{E}_t \, d\rho dz$$

$$+\iint_S \frac{jm}{\rho}\vec{F}_t \cdot \left[\mu_r^{-1}\vec{\nabla}_t(\rho E_\varphi)\right] \, d\rho dz$$

$$+\iint_S \frac{m^2}{\rho}\vec{F}_t \cdot (\mu_r^{-1}\vec{E}_t) \, d\rho dz$$

$$+j\omega\mu_0\sum_{p=1}^2 \int_{L_p} \rho(\vec{F}_t \times \vec{H}_\varphi) \cdot \vec{i}_p d\rho = 0. \tag{5}$$

where F_φ and $\vec{F}_t$ are testing functions. The computational domain S is bounded by L, which consists of two ports, L_1 and L_2, the axis of the structure L_a and the waveguide boundary L_b (see Fig.2). The unit vectors $\vec{i}_p$ are normal (outside) to the ports' cross sections, and functions $\vec{H}_t^p$ and $\vec{H}_\varphi^p$ represent excitation in these ports.

A. Calculation of Scattering Parameters with the Use of GIM

The main idea of the GIM is based on finding the relation between the electric and magnetic fields at the ports of the structure. Let us assume that the fields at the ports are
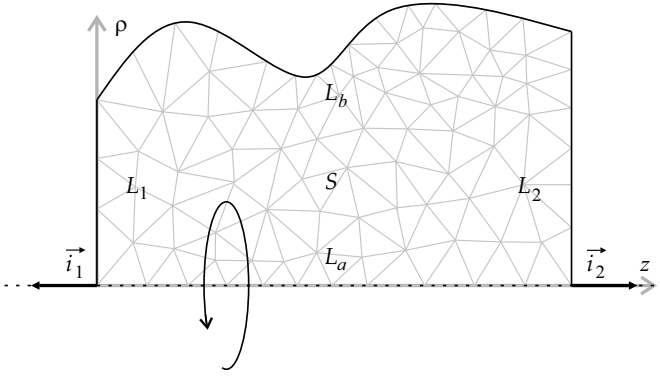
Fig. 2. Example of a two-dimensional computational domain for BOR combined with FEM.

expressed by the modal basis obtained for the regular circular waveguide

$$\vec{E}_\xi^p = \sum_{q=1}^Q (V_q^{TE,p} \vec{e}_{\xi,q}^{TE,p} + V_q^{TM,p} \vec{e}_{\xi,q}^{TM,p}), \tag{6}$$

$$\vec{H}_\xi^p = \sum_{q=1}^Q (I_q^{TE,p} \vec{h}_{\xi,q}^{TE,p} + I_q^{TM,p} \vec{h}_{\xi,q}^{TM,p}), \tag{7}$$

where Q is the number of modes considered in the ports, $p = \{1, 2\}$ is a port number, and $\vec{e}_{\xi,q}^{(\cdot),p}$ and $\vec{h}_{\xi,q}^{(\cdot),p}$ are defined in Appendix A for $\xi = \{t, \varphi\}$. In such a case any electric field at the ports is unambiguously defined by the set of coefficients $\mathbf{V} = [\mathbf{V^1}, \mathbf{V^2}]^T$, where

$$\mathbf{V^P} = [V_1^{TE,p}, \ldots, V_Q^{TE,p}, V_1^{TM,p}, \ldots, V_Q^{TM,p}]^T \tag{8}$$

and similarly a magnetic field by set $\mathbf{I} = [\mathbf{I^1}, \mathbf{I^2}]^T$, where

$$\mathbf{I^P} = [I_1^{TE,p}, \ldots, I_Q^{TE,p}, I_1^{TM,p}, \ldots, I_Q^{TM,p}]^T. \tag{9}$$

Hence, the GIM represented by matrix $\mathbf{Z}$ is the relation between these coefficients:

$$\mathbf{V} = \mathbf{ZI}. \tag{10}$$

In order to obtain this matrix the FEM can be utilized, as has been widely described in the literature [33], [36].

Let us assume that the electric field in the discretized region can be expressed utilizing standard hierarchical (scalar and vector) basis functions [37] $\alpha_{(\cdot)}^{[n]}$ and $\vec{W}_{(\cdot)}^{[n]}$ of the second order:

$$E_\varphi = \sum_{n=1}^N \sum_{i=1}^6 \Psi_{(i)}^{[n]} \alpha_{(i)}^{[n]}, \quad \vec{E}_t = \sum_{n=1}^N \sum_{i=1}^8 \Phi_{(i)}^{[n]} \vec{W}_{(i)}^{[n]}, \tag{11}$$

where $n = 1, \ldots, N$ is the element number with N being the total number of elements, i represents the local node/edge, and $\Psi_{(i)}^{[n]}$ and $\Phi_{(i)}^{[n]}$ are unknown coefficients for the scalar and vector components, respectively. Starting from the weak form of the problem (4) and (5) a simple system of equations can be obtained (in analogy to [33]):

$$\mathbf{G} \begin{bmatrix} \mathbf{\Phi} \\ \mathbf{\Psi} \end{bmatrix} = j\omega\mu_0 \mathbf{BI}, \tag{12}$$

where global matrices $\mathbf{G}$ and $\mathbf{B}$ can be obtained from the aggregation of proper local matrices [33]:

$$\mathbf{G}^{[n]} = \begin{bmatrix} \mathbf{G}_{t,t}^{[n]} & \mathbf{G}_{t,\varphi}^{[n]} \\ \mathbf{G}_{\varphi,t}^{[n]} & \mathbf{G}_{\varphi,\varphi}^{[n]} \end{bmatrix} \tag{13}$$

and

$$\mathbf{B}^{[n]} = \begin{bmatrix} \mathbf{B}_{t,TE}^{[n],1} & \mathbf{B}_{t,TM}^{[n],1} & \mathbf{B}_{t,TE}^{[n],2} & \mathbf{B}_{t,TM}^{[n],2} \\ \mathbf{B}_{\varphi,TE}^{[n],1} & \mathbf{B}_{\varphi,TM}^{[n],1} & \mathbf{B}_{\varphi,TE}^{[n],2} & \mathbf{B}_{\varphi,TM}^{[n],2} \end{bmatrix}, \tag{14}$$

where the submatrices are described in Appendix B.

From the projection of the electric field at the ports on the basis (7), another simple system of equations can be obtained

$$\mathbf{B}^H \begin{bmatrix} \mathbf{\Phi} \\ \mathbf{\Psi} \end{bmatrix} = \mathbf{\Delta V}, \tag{15}$$

where

$$\mathbf{\Delta} = diag\{\Delta_1^{TE}, \Delta_2^{TE}, \ldots, \Delta_1^{TM}, \Delta_2^{TM}, \ldots\} \tag{16}$$

and

$$\Delta_q^{(\cdot)} = \int_L \left(\vec{e}_{t,q}^{(\cdot)} + \vec{e}_{\varphi,q}^{(\cdot)} \right) \cdot \left(\vec{h}_{t,q}^{(\cdot)} + \vec{h}_{\varphi,q}^{(\cdot)} \right)^* \rho d\rho. \tag{17}$$

Finally, the relations (12) and (15) can be combined into a single formula:

$$j\omega\mu_0 \mathbf{B}^H \mathbf{G}^{-1} \mathbf{BI} = \mathbf{\Delta V}, \tag{18}$$

which determines the GIM as follows:

$$\mathbf{Z} = j\omega\mu_0 \mathbf{\Delta}^{-1} \mathbf{B}^H \mathbf{G}^{-1} \mathbf{B}. \tag{19}$$

From the above GIM $\mathbf{Z}$, a multi-mode scattering matrix $\mathbf{S}$ of the waveguide section can be obtained [38]. Both $\mathbf{Z}$ and $\mathbf{S}$ are of dimensions $4Q \times 4Q$ (Q modes for TE and TM for each port). Next, such a matrix can be utilized to construct more complicated structures composed of the same or different sections (eg. periodic/quasi-periodic structures or waveguide filters). In the case of periodic structures, the simple rule described in [39] can be applied to find the structure propagation coefficients from the scattering matrix of a unit cell, which boils down to solving a matrix eigenvalue problem with respect to the propagation coefficient. In the case of other filtering structures, a cascading formula of multimode scattering matrices [40] can be utilized to calculate the structure responses.

B. Periodic Boundary Conditions with No Sources

In some cases, especially for periodic structures with short unit cell sections with complex geometry, the approach presented in the previous paragraph can be inefficient or even ineffective due to the huge number of modes required to properly describe a waveguide section. In such a case, the scattering matrix can be numerically ill-conditioned and it is better to introduce periodic boundary condition (PBC), which does not involve modal expression of the fields in the ports.

The implementation of PBC is based on the elimination of the sources in (12)

$$\mathbf{G} \begin{bmatrix} \mathbf{\Phi} \\ \mathbf{\Psi} \end{bmatrix} = 0 \tag{20}$$

and requires a rearrangement of the unknown variables in vectors $\mathbf{\Phi}$ and $\mathbf{\Psi}$ (similarly to the approach proposed in [21]). The fields at the left port (L_1) are denoted by $\mathbf{\Phi}_L$ and $\mathbf{\Psi}_L$, whereas at the right port (L_2) by $\mathbf{\Phi}_R$ and $\mathbf{\Psi}_R$. Moreover, they are linked by the following relation

$$\begin{bmatrix} \mathbf{\Phi}_R \\ \mathbf{\Psi}_R \end{bmatrix} = \begin{bmatrix} \mathbf{\Phi}_L \\ \mathbf{\Psi}_L \end{bmatrix} e^{-\gamma p}, \tag{21}$$

where $\gamma = \alpha + j\beta$ represents the propagation coefficient and p the length of the unit cell (the period). The other elements of the vectors $\mathbf{\Phi}$ and $\mathbf{\Psi}$ must also be segregated into two groups. The first one contains fields inside the numerical domain $\mathbf{\Phi}_I$ and $\mathbf{\Psi}_I$, the second one fields at the boundary described by Dirichlet conditions $\mathbf{\Phi}_D$ and $\mathbf{\Psi}_D$ (which eventually can be neglected). Finally, the system (20) can be reformulated to a more convenient matrix equation:

$$\begin{bmatrix} \mathbf{G}_{II} & \mathbf{G}_{IL} & \mathbf{G}_{IR} & \mathbf{G}_{ID} \\ \mathbf{G}_{LI} & \mathbf{G}_{LL} & \mathbf{G}_{LR} & \mathbf{G}_{LD} \\ \mathbf{G}_{RI} & \mathbf{G}_{RL} & \mathbf{G}_{RR} & \mathbf{G}_{RD} \\ \mathbf{G}_{DI} & \mathbf{G}_{DL} & \mathbf{G}_{DR} & \mathbf{G}_{DD} \end{bmatrix} \begin{bmatrix} \mathbf{\Phi}_I \\ \mathbf{\Psi}_I \\ \mathbf{\Phi}_L \\ \mathbf{\Psi}_L \\ \mathbf{\Phi}_R \\ \mathbf{\Psi}_R \\ \mathbf{\Phi}_D \\ \mathbf{\Psi}_D \end{bmatrix} = 0. \tag{22}$$

After some algebra, involving relation (21), the above system can be reduced to a simple generalized matrix eigenvalue problem

$$\begin{bmatrix} \mathbf{G}_{II}\,\mathbf{G}_{IL} \\ \mathbf{G}_{RI}\ \ 0 \end{bmatrix} \begin{bmatrix} \mathbf{\Phi}_I \\ \mathbf{\Psi}_I \\ \mathbf{\Phi}_L \\ \mathbf{\Psi}_L \end{bmatrix} = -e^{-\gamma p} \begin{bmatrix} \mathbf{0} & \mathbf{G}_{IR} \\ \mathbf{G}_{LI} & \mathbf{G}_{LL}+\mathbf{G}_{RR} \end{bmatrix} \begin{bmatrix} \mathbf{\Phi}_I \\ \mathbf{\Psi}_I \\ \mathbf{\Phi}_L \\ \mathbf{\Psi}_L \end{bmatrix}. \tag{23}$$

A solution of this problem provides the characteristic dispersion of the considered mode and the corresponding field distribution inside the structure.

III. NUMERICAL RESULTS

In order to confirm the validity of the proposed approach three structures of different geometries were examined (see Fig. 3). The algorithm was implemented in the Matlab environment, and all of the tests were performed using an Intel(R) Core i7-2600K CPU 3.40 GHz, 16 GB RAM computer. The results were validated by comparison with those obtained from commercial software and the literature.

The first considered structure was a periodic waveguide whose axial cross sections are presented in Fig. 3(a), and the dimensions are $p = 13.1125$ mm, $a = 50$ mm, $p_1 = 2.6225$ mm, $p_2 = 7.8675$ mm, $h_1 = 2.025$ mm and $h_2 = 6.075$ mm. The structure is presented in [6], however only for $m = 0$ since the authors claim that a two-dimensional analysis is not sufficient for $m \neq 0$ and it requires three dimensional discretization. As is shown here, this requirement is unnecessary and the dispersion characteristics (for different values of m) obtained from the proposed approach are presented in Fig. 4. The simulation was performed for a 2D mesh composed of $N = 2416$ triangular elements involving PBC and GIM
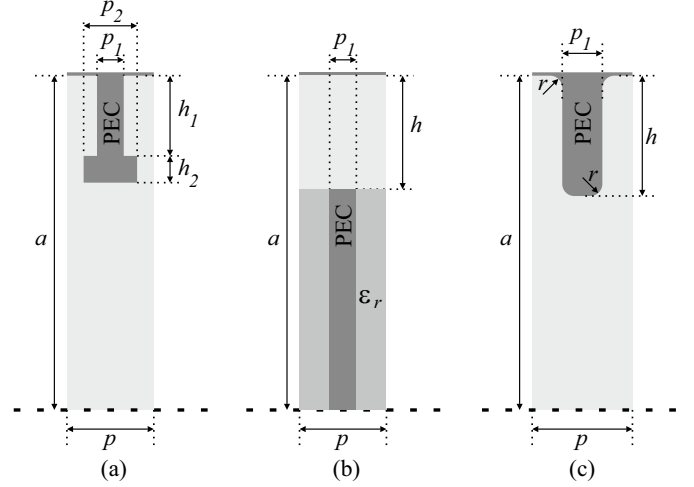

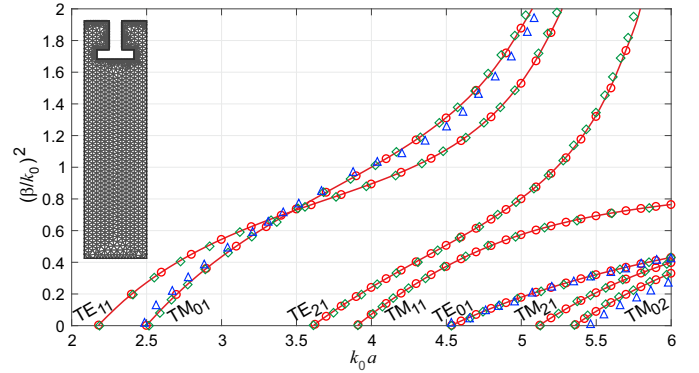Fig. 3. Axial cross sections of single cells in the considered structures.

Fig. 4. Dispersion characteristics of periodic structure composed of cells presented in Fig. 3(a) (GIM - red line, PBC - red circles, HFSS - green diamonds, [6] - blue triangles).

approaches, with the use of $Q = 10$ modes for GIM, which was sufficient to obtain accurate results. The increase of mesh density and number of modes does not significantly reduce the convergence error but increases the analysis time. The results are compared with those obtained from the HFSS 3D commercial software and with those from [6] for $m = 0$. All of the results are in excellent agreement, however the computational time of 2D analysis was shorter by about two orders of magnitude than the full 3D simulation.

As the second example, a dielectric and metal-loaded periodic circular waveguide [8] was considered (see Fig. 3(b)) for two different unit cell lengths p. The dimensions of this structure are as follows $a = 9$ mm, $h = 3$ mm, $p = 0.5$ mm or $p = 10$ mm, $p_1 = 0.1p$ and the relative permittivity of the dielectric is $\varepsilon_r = 15$. In the cases of $p = 0.5$ mm, due to the short length of the unit cell, the approach involving GIM is ineffective. The high complexity of the fields at the ports requires a huge number of modes and the computation of the scattering matrix can be numerically ill-conditioned so it is better to introduce PBC, which does not involve modal expressions of the fields in the ports. The results presented in Fig. 5 obtained in the analysis involving PBC (with $N = 1060$ for $p = 0.5$ mm triangular elements - see
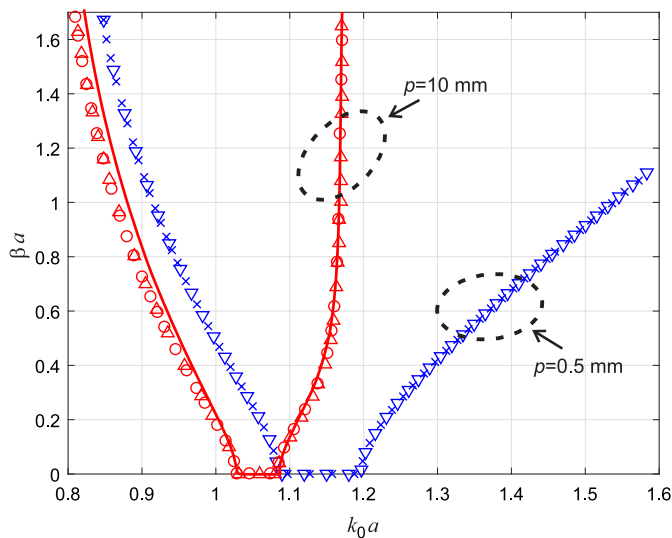
Fig. 5. Dispersion characteristics of periodic structure composed of cells presented in Fig. 3(b) for different unit cell lengths: $p = 0.5$ mm (PBC - crosses, [8] - downward pointing triangles), $p = 10$ mm (GIM - solid line, PBC - circles, [8] - upward pointing triangles).
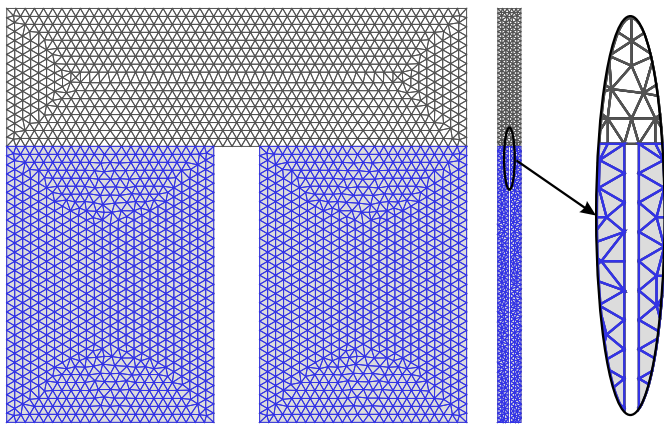

Fig. 6. Meshes for the structure presented in Fig. 3(b) for different unit cell lengths: $p = 10$ mm and $p = 0.5$ mm.

Fig. 6) are in excellent agreement with those obtained with the mode matching technique and verified experimentally in [8]. For longer cells ($p = 10$ mm) in the periodic structures it was sufficient to utilize $Q = 10$ modes for GIM analysis to obtain consistent results (with $N = 4799$ triangular elements).

The last structure was a corrugated empty waveguide with rounded edges, as is shown in Fig. 3(c). Such common guides are usually considered only for sharp edges [4] even though the roundings are very important from a practical point of view (for example, due to the manufacturing technology or high power transmission). The analysis was performed for $a = 25$ mm, $h = 11$ mm, $d = 5$ mm, $p = 15$ mm and different values of radii: $r = 0$ mm (with $N = 1561$ triangular elements) and $r = 2.38$ mm (with $N = 1850$ triangular elements). The scattering matrix for ($Q = 6$ modes) obtained using the GIM approach agrees very well with the one from the 3D InventSim analysis - scattering parameters for TE_{11} are
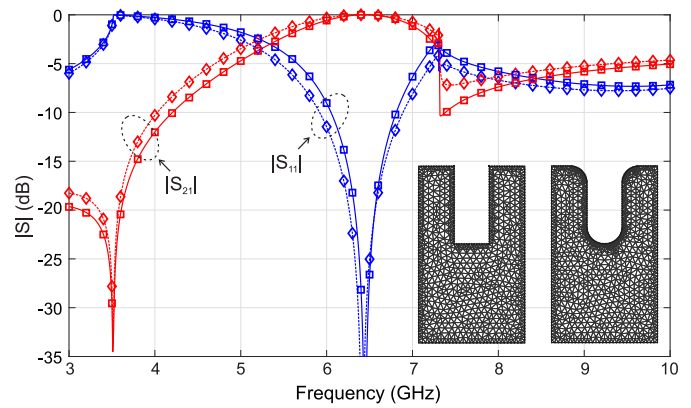

Fig. 7. Scattering parameters of TE_{11} mode for a single cell from Fig. 3(c) and different rounding radii: $r = 0$ mm (GIM - solid line, InventSim - squares), $r = 2.38$ mm (GIM - dashed line, InventSim - diamonds).
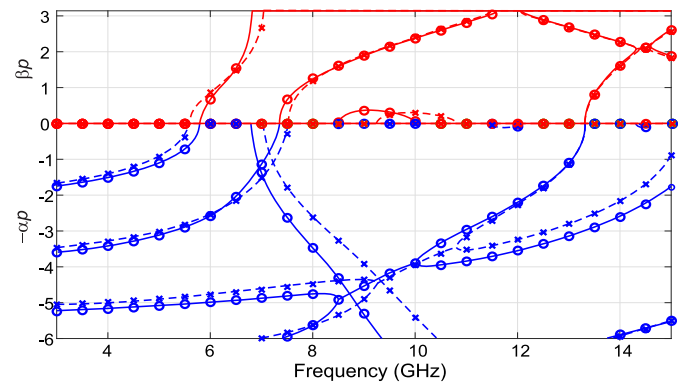

Fig. 8. Normalized propagation coefficients versus frequency for the periodic structure from Fig. 3(c) and different rounding radii: $r = 0$ mm (GIM - solid line, PBC - circles), $r = 2.38$ mm (GIM - dashed line, PBC - crosses).

presented in Fig. 7. Also, the results obtained in the analysis of the periodic structure involving both GIM and PBC methods are in excellent agreement (see Fig. 8). As can be seen, the roundings can significantly affect the dispersion characteristics of this simple structure (e.g. modifying its bands). Similarly to the previous examples the computation time in the case of 2D analysis was about two orders of magnitude shorter than in commercial software.

IV. CONCLUSION

A two-dimensional FEM has been utilized to investigate axially symmetrical guiding structures. The utilization of BOR significantly improves the efficiency of the discrete analysis reducing the computational time by up to two orders of magnitude. This attribute makes this technique comparable to the analytical approaches while maintaining great flexibility of the algorithm with respect to structure geometry. The proposed approaches allow the study of periodic/quasi-periodic structures as well as whole devices composed of different waveguide sections. The validity and efficiency of the presented technique have been verified, which confirms its usefulness for the design and optimization process.

APPENDIX A
THE ELECTRIC AND MAGNETIC FIELDS IN A HOMOGENEOUS CIRCULAR WAVEGUIDE

In order to create a proper basis (7) for GIM definition the following field distributions in a homogeneous circular waveguide are required. For TE modes:

$$\vec{e}_{t,q}^{TE,p} = \frac{\omega\mu m}{\kappa_q'^2\rho} J_m(\kappa_q'\rho)\vec{i}_\rho,$$

$$\vec{e}_{\varphi,q}^{TE,p} = \frac{j\omega\mu}{\kappa_q'} J_m(\kappa_q'\rho)\vec{i}_\varphi,$$

$$\vec{h}_{t,q}^{TE,p} = -\frac{\gamma_q'}{\kappa_q'} J_m'(\kappa_q'\rho)\vec{i}_\rho + J_m(\kappa_q'\rho)\vec{i}_z,$$

$$\vec{h}_{\varphi,q}^{TE,p} = -\frac{jm\gamma_q'}{\kappa_q'^2\rho} J_m'(\kappa'_q\rho)\vec{i}_\varphi$$

and for TM modes:

$$\vec{e}_{t,q}^{TM,p} = -\frac{\gamma_q}{\kappa_q} J_m'(\kappa_q\rho)\vec{i}_\rho + J_m(\kappa_q\rho)\vec{i}_z,$$

$$\vec{e}_{\varphi,q}^{TM,p} = -\frac{jm\gamma_q}{\kappa_q^2\rho} J_m(\kappa_q\rho)\vec{i}_\varphi,$$

$$\vec{h}_{\varphi,q}^{TM,p} = -\frac{j\omega\varepsilon}{\kappa_q} J_m'(\kappa_q\rho)\vec{i}_\varphi,$$

$$\vec{h}_{t,q}^{TM,p} = -\frac{m\omega\varepsilon}{\kappa_q^2\rho} J_m(\kappa_q\rho)\vec{i}_\rho.$$

Parameters κ_q and κ_q' represent the sequential roots of the Bessel function of order m and the roots of its derivative, respectively, divided by the waveguide radius.

APPENDIX B
DETAILED FORM OF THE LOCAL FEM MATRICES

The local matrices in equation (13) have the following form:

$$\left[\mathbf{G}_{t,t}^{[n]}\right]_{k,i} = \iint_{S^{[n]}} \left(\vec{\nabla}_t \times \vec{W}_{(k)}^{[n]}\right) \cdot \left(\mu_r^{-1}\vec{\nabla}_t \times \vec{W}_{(i)}^{[n]}\right) \rho d\rho dz$$

$$-k_0^2 \iint_{S^{[n]}} \vec{W}_{(k)}^{[n]} \cdot \bar{\varepsilon}_r \vec{W}_{(i)}^{[n]} \,\rho d\rho dz$$

$$+ \iint_{S^{[n]}} \frac{m^2}{\rho} \vec{W}_{(k)}^{[n]} \cdot \left(\mu_r^{-1}\vec{W}_{(i)}^{[n]}\right) d\rho dz,$$

$$\left[\mathbf{G}_{t,\varphi}^{[n]}\right]_{k,i} = \iint_{S^{[n]}} \frac{jm}{\rho} \vec{W}_{(k)}^{[n]} \cdot \left(\mu_r^{-1}\vec{\nabla}_t(\rho\alpha_{(i)}^{[n]})\right) d\rho dz,$$

$$\left[\mathbf{G}_{\varphi,\varphi}^{[n]}\right]_{k,i} = \iint_{S^{[n]}} \frac{1}{\rho} \vec{\nabla}_t(\rho\alpha_{(k)}^{[n]}) \cdot \left(\mu_r^{-1}\vec{\nabla}_t(\rho\alpha_{(i)}^{[n]})\right) d\rho dz$$

$$-k_0^2 \iint_{S^{[n]}} \alpha_{(k)}^{[n]} \varepsilon_r \alpha_{(i)}^{[n]} \rho d\rho dz,$$

$$\left[\mathbf{G}_{\varphi,t}^{[n]}\right]_{k,i} = -\iint_{S^{[n]}} \frac{jm}{\rho} \vec{\nabla}_t(\rho\alpha_{(k)}^{[n]}) \cdot \mu_r^{-1}\vec{W}_{(i)}^{[n]} d\rho dz,$$

whereas local matrices in (14) are defined by

$$\left[\mathbf{B}_{t,TE}^{[n],p}\right]_{k,q} = \int_{L\cap L^{[n]}} \vec{W}_{(k)}^{[n]} \cdot (\vec{i}_p \times \vec{h}_{\varphi,q}^{TE,p})\rho d\rho,$$

$$\left[\mathbf{B}_{t,TM}^{[n],p}\right]_{k,q} = \int_{L\cap L^{[n]}} \vec{W}_{(k)}^{[n]} \cdot (\vec{i}_p \times \vec{h}_{\varphi,q}^{TM,p})\rho d\rho,$$

$$\left[\mathbf{B}_{\varphi,TE}^{[n],p}\right]_{k,q} = \int_{L\cap L^{[n]}} \alpha_{(k)}^{[n]}\vec{i}_\varphi \cdot (\vec{i}_p \times \vec{h}_{t,q}^{TE,p})\rho d\rho,$$

$$\left[\mathbf{B}_{\varphi,TM}^{[n],p}\right]_{k,q} = \int_{L\cap L^{[n]}} \alpha_{(k)}^{[n]}\vec{i}_\varphi \cdot (\vec{i}_p \times \vec{h}_{t,q}^{TM,p})\rho d\rho.$$

REFERENCES

[1] C.-J. Lai, C.-I. Hsu, C.-H. Lee, and J.-F. Kiang, "Dispersion properties of circular dielectric waveguides loaded with periodic metal disks," *Microw. Opt. Technol. Lett.*, vol. 49, no. 9, pp. 2057–2061, Sept. 2007.

[2] J. Bornemann and S. Y. Yu, "Novel designs of polarization-preserving circular waveguide filters," *Int. J. Microw. Wirel. Technol.*, vol. 2, no. 6, pp. 531–536, Dec. 2010.

[3] S. Amari and J. Bornemann, "Design of polarization-preserving circular waveguide filters with attenuation poles," *Microw. Opt. Technol. Lett.*, vol. 31, no. 5, pp. 334–336, Dec. 2001.

[4] J. Bornemann and S. Y. Yu, "Circular waveguide tm 11-mode resonators and their application to polarization-preserving bandpass and quasi-highpass filters," in *German Microwave Conference Digest of Papers*. IEEE, Apr. 2010, pp. 202–205.

[5] M.-S. Tong, R. Sauleau, A. Rolland, and T.-G. Chang, "Analysis of electromagnetic band-gap waveguide structures using body-of-revolution finite-difference time-domain method," *Microw. Opt. Technol. Lett.*, vol. 49, no. 9, pp. 2201–2206, Sept. 2007.

[6] L. Kuhler, G. Le Fur, L. Duchesne, and N. Raveu, "The propagation characteristics of 2-d metamaterial waveguides using the modal expansion theory," *IEEE Trans. Microw. Theory Tech.*, vol. 66, no. 10, pp. 4319–4326, Aug. 2018.

[7] S. Amari, R. Vahldieck, J. Bornemann, and P. Leuchtmann, "Spectrum of corrugated and periodically loaded waveguides from classical matrix eigenvalues," *IEEE Trans. Microw. Theory Tech.*, vol. 48, no. 3, pp. 453–460, Mar. 2000.

[8] A. Kusiek and J. Mazur, "Left-handed propagation characteristics of a dielectric and metal-loaded periodic circular waveguide," *J. Electromagn. Waves Appl.*, vol. 31, no. 16, pp. 1698–1710, 2017.

[9] M. Aghadjani and P. Mazumder, "Thz polarizer controller based on cylindrical spoof surface plasmon polariton (c-sspp)," *IEEE Trans. Terahertz Sci. Technol.*, vol. 5, no. 4, pp. 556–563, Jul. 2015.

[10] J. P. Leite Neto and J. J. Barroso, "The sinusoid as the longitudinal profile in backward-wave oscillators of large cross sectional area," *Braz. J. Phys.*, vol. 34, no. 4B, pp. 1577–1582, Dec. 2004.

[11] A. Ashrafi, A. Hasanbeigi, and H. Mehdian, "Dispersion and growth characteristics in a circular waveguide loaded with alternate metal and dielectric discs," *AIP Adv.*, vol. 8, no. 1, p. 015322, Jan. 2018.

[12] M. T. et al., "Cad of complex passive devices composed of arbitrarily shaped waveguides using nystro/spl uml/m and bi-rme methods," *IEEE Trans. Microw. Theory Tech.*, vol. 53, no. 6, pp. 2153–2163, Jun. 2005.

[13] M. B. M. Bressan, S. Battistutta and L. Perregrini, "Modeling of inhomogeneous and lossy waveguide components by the segmentation technique combined with the calculation of green's function by ewald's method," *IEEE Trans. Microw. Theory Tech.*, vol. 66, no. 2, pp. 633–642, Jan. 2018.

[14] D. M. Shyroki, "Efficient cartesian-grid-based modeling of rotationally symmetric bodies," *IEEE Trans. Microw. Theory Tech.*, vol. 55, no. 6, pp. 1132–1138, Jun. 2007.

[15] B. Fuchs, S. Palud, L. Le Coq, O. Lafond, M. Himdi, and S. Rondineau, "Scattering of spherically and hemispherically stratified lenses fed by any real source," *IEEE Trans. Antennas Propag.*, vol. 56, no. 2, pp. 450–460, Feb. 2008.

[16] E. Jørgensen, P. Meincke, and M. Sabbadini, "Fast and accurate design tool for rotationally symmetric reflector antennas with 3d waveguide components and support structures," in *Proc. 34th ESA Antenna Workshop*, 2012.

[17] V. S. Bulygin, T. M. Benson, Y. V. Gandel, and A. I. Nosich, "Full-wave analysis and optimization of a tara-like shield-assisted paraboloidal reflector antenna using a nystrom-type method," *IEEE Trans. Antennas Propag.*, vol. 61, no. 10, pp. 4981–4989, Oct. 2013.

[18] J. Chen, J. Wang, and C. Tian, "Using weakly conditionally stable-body of revolution-finite-difference time-domain method to simulate dielectric film-coated circular waveguide," *IET Microw. Antennas Propag.*, vol. 9, no. 9, pp. 853–860, Jun. 2015.

[19] G. P. Zouros and G. C. Kokkorakis, "Electromagnetic scattering by an inhomogeneous gyroelectric sphere using volume integral equation and orthogonal dini-type basis functions," *IEEE Trans. Antennas Propag.*, vol. 63, no. 6, pp. 2665–2676, Jun. 2015.

[20] M. Celuch and W. K. Gwarek, "Industrial design of axisymmetrical devices using a customized fdtd solver from rf to optical frequency bands [application notes]," *IEEE Microw. Mag.*, vol. 9, no. 6, pp. 150–159, Dec. 2008.

[21] J.-M. Jin, *The finite element method in electromagnetics*. John Wiley & Sons, 2015.

[22] A. D. Greenwood and J.-M. Jin, "Finite-element analysis of complex axisymmetric radiating structures," *IEEE Trans. Antennas Propag.*, vol. 47, no. 8, pp. 1260–1266, Aug. 1999.

[23] E. A. Dunn, J.-K. Byun, E. D. Branch, and J.-M. Jin, "Numerical simulation of bor scattering and radiation using a higher order fem," *IEEE Trans. Antennas Propag.*, vol. 54, no. 3, pp. 945–952, Mar. 2006.

[24] G. Gentili, P. Bolli, R. Nesti, G. Pelosi, and L. Toso, "High-order fem mode matching analysis of circular horns with rotationally symmetric dielectrics," *IEEE Trans. Antennas Propag.*, vol. 55, no. 10, pp. 2915–2918, Oct. 2007.

[25] J.-M. Jin, Z. Lou, Y.-J. Li, N. W. Riley, and D. J. Riley, "Finite element analysis of complex antennas and arrays," *IEEE Trans. Antennas Propag.*, vol. 56, no. 8, pp. 2222–2240, Aug. 2008.

[26] M. M. Ilic, A. Z. Ilic, and B. M. Notaros, "Continuously inhomogeneous higher order finite elements for 3-d electromagnetic analysis," *IEEE Trans. Antennas Propag.*, vol. 57, no. 9, pp. 2798–2803, Sept. 2009.

[27] X. Rui, J. Hu, and Q. H. Liu, "Higher order finite element method for inhomogeneous axisymmetric resonators," *Prog. Electromagn. Res.*, vol. 21, pp. 189–201, 2010.

[28] Y. B. Zhai, X. W. Ping, X. Y. Zhou, J. F. Zhang, W. M. Yu, W. B. Lu, and T. J. Cui, "Fast computations to electromagnetic scattering properties of complex bodies of revolution buried and partly buried in layered lossy media," *IEEE Trans. Geosci. Remote Sens.*, vol. 49, no. 4, pp. 1431–1440, Apr. 2011.

[29] D.-Y. Na, B.-H. V. Borges, and F. L. Teixeira, "Finite element time-domain body-of-revolution maxwell solver based on discrete exterior calculus," *J. Comput. Phys.*, vol. 376, pp. 249–275, Jan. 2019.

[30] R. N. G. P. G. G. Gentili, M. Khosronejad and S. Selleri, "An efficient 2.5-d finite-element approach based on transformation optics for the analysis of elliptical horns," *IEEE Trans. Antennas Propag.*, vol. 66, no. 9, pp. 4782–4790, Sept. 2018.

[31] G. P. S. S. G. G. Gentili, M. Khosronejad, "Analysis of elliptical structures with constant axial ratio by body-of-revolution finite element method and transformation optics," *Int. J. Microw. Wirel. Technol.*, pp. 501–508, Jun. 2019.

[32] M. Czarniewska, G. Fotyga, A. Lamecki, and M. Mrozowski, "Parametrized local reduced-order models with compressed projection basis for fast parameter-dependent finite-element analysis," *IEEE Trans. Microw. Theory Tech.*, vol. 66, no. 8, pp. 3656–3667, Jun. 2018.

[33] P. Kowalczyk, R. Lech, M. Warecka, and A. Kusiek, "Electromagnetic plane wave scattering from a cylindrical object with an arbitrary cross section using a hybrid technique," *J. Electromagn. Waves Appl.*, vol. 33, no. 2, pp. 178–192, 2018.

[34] J. Rubio, J. Arroyo, and J. Zapata, "Analysis of passive microwave circuits by using a hybrid 2-D and 3-D finite-element mode-matching method," *IEEE Trans. Microw. Theory Tech.*, vol. 47, no. 9, pp. 1746–1749, Sept. 1999.

[35] A. Lamecki, "A Mesh Deformation Technique Based on Solid Mechanics for Parametric Analysis of High-Frequency Devices With 3-D FEM," *IEEE Trans. Microw. Theory Tech.*, vol. 64, no. 11, pp. 3400–3408, Nov. 2016.

[36] J. Rubio, M. González, and J. Zapata, "Analysis of cavity-backed microstrip antennas by a 3-D finite element segmentation method and a matrix Lanczos-Padé algorithm (SFELP)," *IEEE Antennas Wireless Propag. Lett.*, vol. 1, pp. 193–195, 2002.

[37] D. B. Davidson, *Computational Electromagnetics for RF and Microwave Engineering*. Cambridge university press, 2005.

[38] D. M. Pozar, *Microwave engineering*. John Wiley & Sons, 2009.

[39] R. Lech and J. Mazur, "Propagation in rectangular waveguides periodically loaded with cylindrical posts," *IEEE Microw. Wireless Compon. Lett.*, vol. 14, no. 4, pp. 177–179, May 2004.

[40] J. Uher, J. Bornemann, and U. Rosenberg, *Waveguide components for antenna feed systems: Theory and CAD*. Artech House Publishers, 1993.

Malgorzata Warecka received the MScEE degree from the Gdansk University of Technology, Gdansk, Poland, in 2018 where she is currently working toward the PhD degree. She is currently with the Faculty of Electronics, Telecommunications and Informatics, Department of Microwave and Antenna Engineering, Gdansk University of Technology. Her current research interests include scattering and propagation of electromagnetic wave problems, algorithms, and numerical methods.

Rafal Lech (M'14-SM'17) was born in Elblag, Poland, in 1977. He received the M.Sc.E.E., Ph.D. (with honors) and D.Sc. degrees from the Gdansk University of Technology, Gdansk, Poland, in 2001, 2007 and 2018, respectively. He is currently with the Department of Microwave and Antenna Engineering, Faculty of Electronics, Telecommunications and Informatics, Gdansk University of Technology. His main research interests are electromagnetic wave scattering, hybrid methods, filter design, complex materials, metamaterial applications at microwave frequencies, electromagnetic analysis of periodic structures and antenna design.

Piotr Kowalczyk (M'19) was born in Wejherowo, Poland, in 1977. He received the M.Sc.E.E. degree in applied physics and mathematics, Ph.D. (with honors) and D.Sc. degrees in electrical engineering from the Gdansk University of Technology, Gdansk, Poland, in 2001, 2008 and 2018, respectively. He is currently with the Faculty of Electronics, Telecommunications and Informatics, Department of Microwave and Antenna Engineering, Gdansk University of Technology. His current research interests include scattering and propagation of electromagnetic wave problems, algorithms, and numerical methods.